Pergamon

Solid State Communications, Vol. 101, No. 8, pp. 575–580, 1997

0038–1098/97 $17.00+.00

PII: S0038-1098(96)00663-1

SYNCHROTRON RADIATION PHOTOEMISSION STUDY OF THE PASSIVE LAYERS OF HEAT TREATED Fe_3Al-TYPE ALLOY

M.F. López, A. Gutiérrez, M.C. García-Alonso and M.L. Escudero

Departamento de Corrosión y Protección, Centro Nacional de Investigaciones Metalúrgicas, C.S.I.C., Avda. Gregorio del Amo 8, Madrid 28040, Spain

(*Received* 2 *July* 1996; accepted 25 *October* 1996 *by F. Ynduráin*)

We report on a synchrotron radiation photoemission study of an Fe_3Al-type alloy. The influence of different annealing treatments on the surface electronic structure has been investigated. The Al-2*p* photoemission spectra show slight differences among samples with a very small metallic Al component. From the Fe-3*p* and the valence band photoemission spectra, a higher surface Fe-content for the sample having a defective ordered B2 structure is observed. This finding is explained in terms of the bulk structure and the thickness of the passive layer. After determination of the surface composition of the samples, electrochemical experiments in Hank's solution have been performed in order to determine the influence of the passive layer composition on the corrosion behaviour of the samples. The low corrosion rates observed for all specimens indicate that the passive layer formed in air on the material surface gives high corrosion protection to the alloy for all heat treatments. © 1997 Elsevier Science Ltd. All rights reserved

Keywords: A. surfaces and interfaces, D. order–disorder effects, E. photoelectron spectroscopies, E. synchrotron radiation.

Iron aluminides have become materials of great interest since the discovery of their excellent resistance to oxidation [1, 2]. This property as well as its good sulfidation resistance and potentially low material cost have made iron aluminides good candidates in high temperature structural applications. One of the major limitations of these materials is its low room-temperature ductility, a characteristic which has restricted their fabrication and engineering use. This property can be improved by adding Cr up to 6 at% [3–6]. Further improvements in ductility have also been obtained by heavy deformation, for example by rolling, followed by low temperature heat treatments [7–9]. After these advances, a renewed interest on iron aluminides appeared.

Although primarily intended for high-temperature service, these intermetallic alloys may also be suitable for applications where ambient-temperature corrosion resistance is of great importance. Among the novel room temperature applications of these materials can be considered their potential use as biomaterial for surgical implants [10]. Only a few previous studies have examined the room temperature corrosion resistance of iron aluminides and also their improvement with Cr and Mo additions [11–14]. The use of these materials for room temperature applications requires a characterization of their corrosion behaviour.

The Fe_3Al alloy presents two different crystal structures depending on the heat treatment applied: an ordered cubic DO_3 structure and an imperfectly ordered cubic B2 structure [15–17]. A transformation from the DO_3 crystal structure to a defective ordered cubic B2 crystal structure occurs at temperatures above the critical ordering temperature $T_c \approx 550°C$. To evaluate the corrosion resistance of this material, it is essential to study the corrosion behaviour of both crystal structures. Since their mechanical properties have been widely studied, the corrosion study will contribute to a complete characterization of these materials.

The corrosion behaviour of a material in different corrosive media strongly depends on the presence of a protective passive film and, therefore, on the composition of this film. The aim of the present study is to evaluate

the surface composition of Fe_3Al alloy showing different crystal structures by using synchrotron radiation and X-ray photoemission spectroscopy (XPS). To evaluate the influence of the surface composition on the corrosion behaviour of these materials a corrosion characterization by means of electrochemical techniques is performed.

The chemical composition of the studied alloy was 26.6% Al, 4.95% Cr, 0.08% Zr (at%) and remainder Fe. The material was prepared by induction melting and drop casting, followed by hot rolling to strip. At this stage, the material was annealed at 950°C for 30 min and quenched. In order to completely destroy the prior order, strips were cold rolled to a reduction of ~38%. State-A samples (disordered state) were the specimens produced after these conditions. Afterwards, several recrystallization annealing processes were carried out on the heat-treated material, covering a temperature range between 800°C and 500°C. First, state-A samples were annealed at 800°C for 1 h and quenched, giving rise to the state-B material (recrystallized state). The fast quenching after annealing avoids the formation of B2 order in the state-B samples. State-B samples were then annealed at 700°C for 1 h, yielding the state-C samples. During this last annealing, the material is allowed to get an imperfectly ordered B2 structure. Since the critical temperature for DO_3 order in this material is about 540°C, a last anneal below this temperature (at 500°C) for 15 h, followed by air cooling, was performed to obtain the ordered DO_3 phase. Samples produced after this last annealing corresponded to state-D material. Upon each annealing, and to eliminate remaining particles of contamination from rolling and heat treatments, samples were abraded, polished and before testing, ultrasonically cleaned in alcohol. These different material states were selected because their microstructure, mechanical properties and *in vitro* corrosion behaviour had been previously studied [5, 9, 14].

XPS measurements were carried out at the TGM5 monochromator of the Berliner Elektronenspeicherring für Synchrotronstrahlung (BESSY) using undulator light, employing a VSW-ARIES electron spectrometer. The base pressure in the UHV-chamber during measurements was better than 2×10^{-10} mbar. Samples were cleaned by 1 min Ar^+ bombardment at an ion energy of 3 keV.

The corrosion behaviour of the samples was evaluated at room temperature using as electrolyte the Hank's solution, whose composition is given elsewhere [18]. This solution is commonly used for electrochemical studies on biomaterials because its composition is similar to the physiological fluids. For the electrochemical tests, working electrode areas of about 0.78 cm^2 were isolated. A saturated calomel electrode was used as reference, and a platinum wire as counter electrode. The evaluation of the corrosion resistance for each material condition was performed by using the polarization resistance method. The polarization resistance, R_p, is deduced from the expression $R_p = \Delta E/\Delta I$, where ΔE is the potential applied (20 mV) and ΔI is the resulting current for a testing time of about 60 s. After determining the polarization resistance, the corrosion intensities, i_{corr}, can be calculated by applying the well-known Stern-Geary equation ($i_{corr} = B/R_p$), where B is a constant [19]. The pitting corrosion susceptibility was evaluated by means of anodic cyclic polarization curves at a scan rate of 0.16 mV s^{-1}.

Figure 1 shows Al-2p photoemission (PE) spectra at a photon energy of 160 eV for the four Fe_3Al states studied. The spectra were analyzed by a least-squares fitting procedure in order to obtain more information on the chemical state. The experimental data can be approximated by Lorentz curves, representing the different emission lines, convoluted by a Gaussian function, that takes into account the experimental resolution. One Lorentz line was used to describe the Al-2p doublet, corresponding to non-oxidized Al, located at ~72.25 eV. In order to fit the broad spectral feature located at around 75 eV several Lorentz lines were necessary. These lines correspond to Al with different

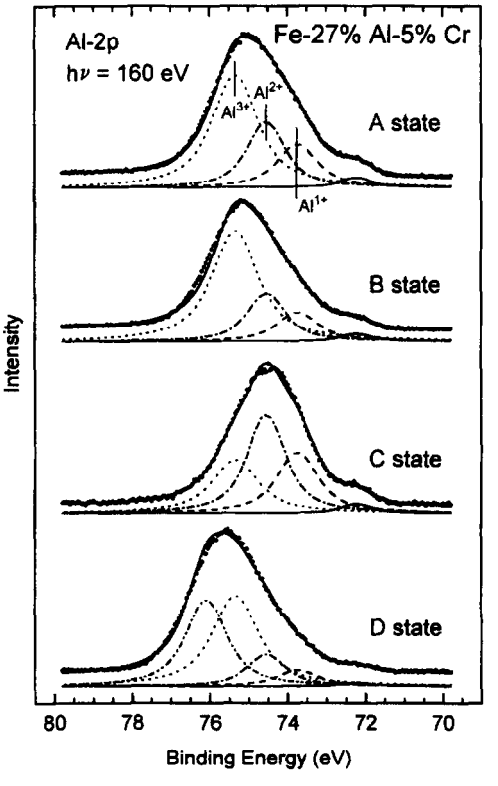

Fig. 1. Al-2p photoemission spectra of the different heat-treated Fe–27%Al–5%Cr alloys. The solid lines through the data points represent the result of the least-square fits. The subspectra show different chemical states of aluminium (see text)

oxidation states. Three different components are needed to well describe the experimental data, which can be assigned to Al^{1+}, Al^{2+} and Al^{3+}. It is not possible to fit the whole peak with a single Lorentz line and three is the minimum to get a satisfactory approximation to the experimental curve. A similar approach, using also three lines, has been made in a very recent work on oxidized Al [20]. The same nomenclature was used in the four spectra of Fig. 1. The dashed subspectra represent the Al^{1+} component located at ~73.75 eV. The dash–dotted curves represent the Al^{2+} component located at ~74.5 eV. The dotted subspectra show the Al^{3+} component at ~75.3 eV. For the state-D it was necessary to use an additional Lorentz line at ~76.10 eV in order to be able to describe the spectrum. The curve is represented by a dash-double-dotted subspectrum and will be commented below. The position and width of the Lorentz lines used in the present analysis are similar to those of [20]. The existence of Al^{1+} and Al^{2+} oxidation states is probably related to the amorphous character of the surface layer which involves a wide distribution of bond lengths and coordination numbers at atomic scale, making possible the existence of Al atoms with low oxidation states. In some previous works [21–24] it has been shown that the Al-2*p* PE oxidized peak changes its binding energy depending on the temperature and oxygen partial pressure. These energy shifts could actually be changes in the intensity ratios between the different oxidation states in amorphous oxidized Al. In particular, in [21] and [22], Venezia *et al.* observed that the position of the oxidized component shifts toward higher binding energies with increasing oxidation temperature. This effect would correspond to an enhancement of the Al^{3+} component produced when the oxidation temperature increases.

As can be observed in Fig. 1, the ratio of the different Al oxidation components is different for each state. The existence of Al^{1+} and Al^{2+} components observed for all samples indicates a partial amorphous character of the Al-rich passive layer, but this amorphous character is different for each sample. Whereas the ratio between the Al^{1+} and Al^{2+} components is approximately constant in all cases, the intensity of the Al^{3+} component as compared to the other oxidation components changes for each state. The intensity of this Al^{3+} component with respect to Al^{2+} can serve as a measure of the amorphous character of the film: the higher the ratio between Al^{3+} and Al^{2+} components, the less amorphous the passive layer. Excluding state-C sample, which has a defect of Al atoms at the surface induced by the structure of the bulk, as will be discussed below, there seems to be a correlation between the amorphous character of the passive film and the structure of the bulk. State-A sample, which has a bulk disordered structure, has the lowest ratio between Al^{3+} and Al^{2+} components, i.e. it has the highest amorphous character. State-B sample, which corresponds to a recrystallized state, presents an intermediate behaviour. Finally, state-D sample with an ordered DO_3 bulk structure has the highest Al^{3+} component as compared to Al^{2+}. These results suggest that the order of the passive layer is directly related to the order of the bulk material. However, state-C sample does not follow this correlation because the defect of Al atoms in the bulk crystal structure induces a thinner passive layer.

An important observation in the spectrum of state-D is the feature found at ~76.2 eV (dash–double-dotted subspectrum), that can not be identified with any other finding in the literature. Its binding energy is too high to be assigned to the previously observed Al^{3+}. Of all possible Al compounds, only in the case of AlF_3 an Al^{3+} 2*p* PE component located at so high binding energy (~76.3 eV) can be found. Fluorine is a very electronegative element and has a tendency to take all electrons from the Al atoms, forming a very ionic compound. Due to the absence of fluorine in the present samples, a possible explanation of this feature could be the existence of atomic dislocations related with positive charges inside the layer that could ionise Al atoms in the same way as fluorine atoms do in the AlF_3 case. The DO_3 crystal structure of the bulk could play an important role, since this feature is only observed for this sample. Nevertheless, we can not find any other explanation to the existence of this new feature.

In the XPS experiments performed at the synchrotron, the Cr-3*p* PE signal could not be observed. This indicates that no significative Cr-diffusion to the surface occurs, i.e., in the formation of the passive layer formation the diffusion of Al towards the surface is the dominating process. In the XPS experiments the Fe-3*p* PE spectral shape observed for all states was quite similar, with a high metallic component at ~53 eV and a smaller oxidized component at ~55 eV. As an example, in the inset of Fig. 2, the Fe-3*p* signal of the state-C sample at a photon energy of 160 eV is represented. The high intensity of the metallic component may indicate that the observed Fe signal does not come from the outermost atomic surface layer, because in that case the oxidized component would be higher than in the present case. This high metallic iron emission probably originates from a metallic bond with Al, which would explain the non-oxidized component observed in the Al-2*p* spectra, located at ~72.25 eV. Since the photon energy used for this experiment was 160 eV, the excited electrons corresponding to the Fe-3*p* emission have kinetic energies of about 107 eV, which corresponds to electrons coming from near the surface [25]. This indicates that the passive layer is very thin, of the order of 2–3 atomic monolayers. Figure 2 shows the intensity of the iron 3*p*

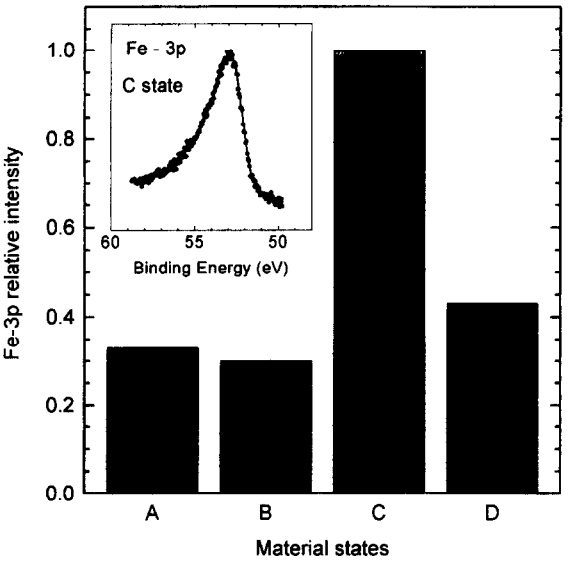

Fig. 2. Fe-3*p* relative intensity obtained for the four different Fe–27%Al–5%Cr alloys. The maximum is given by the state-C material. The inset shows the Fe-3*p* photoemission spectrum for the state-C sample

emission line related to Al-2*p* emission for the four different states. As it can be seen, state-C is the material with the highest Fe-content near the surface. The difference between state C and D can be due to the influence of the crystal structure on the surface composition. As we mentioned above, the material in state-C has a defective ordered cubic B2 crystal structure that corresponds to FeAl, whereas state-D has the ordered DO_3 crystal structure that corresponds to Fe_3Al. Since in both cases we have the same material ratio (26.6 Al at%), the tendency to form FeAl in the bulk B2 structure gives rise to structural vacancies at the Al sites, which can originate a lower diffusion rate of Al atoms. This leads to a thinner passive layer formation and consequently to a relatively higher Fe-content near the surface. The low thickness of the passive layer suggests that the Al oxide in this case (state-C) has not completely evolved towards an equilibrium oxidation state. This explains the high Al^{1+} and Al^{2+} contents as compared to Al^{3+} in Fig. 1.

Figure 3 shows valence-band emission for the four Fe_3Al-type alloy states, for Fe metal and for oxidized Al. The iron aluminides as well as the oxidized Al spectra were taken at a photon energy of 160 eV whereas the Fe metal spectrum was obtained at a photon energy of 100 eV. In the spectra corresponding to the four Fe_3Al-type alloy states, there are three main features, at ≈1 eV, ≈7 eV and ≈10 eV. The first structure is similar to that found in the valence band PE of Fe metal. For oxidized Fe (not shown in Fig. 3) the spectrum obtained is quite similar to that of clean Fe with the same peak at ≈1 eV but also with a small structure at 6 eV [26]. The second

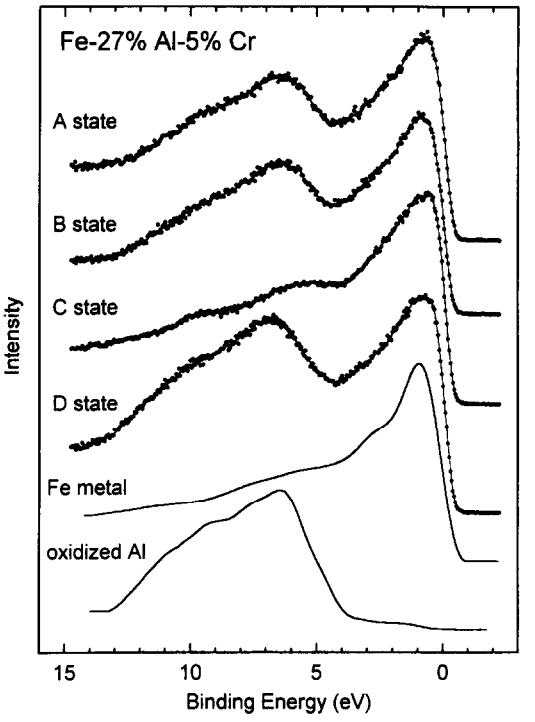

Fig. 3. Valence band photoemission spectra of the different heat-treated Fe–27%Al–5% alloys as well as of a Fe metal sample and an oxidized Al sample

and third peaks are related to the oxidized Al valence band. Figure 3 confirms the higher Fe-content as related to the Al-content at the surface of state-C samples. The XPS results show that all samples have a surface passive layer, rich in aluminium oxide, with some contribution of iron. In order to determine the room temperature corrosion behaviour electrochemical experiments were performed after the composition of the passive film formed in air was determined. Among the possible room temperature applications of these materials, we have considered their potential application as surgical implants. Consequently, we performed the electrochemical measurements in Hank's solution. Figure 4(a) shows the corrosion current densities, i_{corr}, versus testing time deduced from the polarization resistance method for all the Fe_3Al-type alloy states. As it can be seen, the i_{corr} values are quite low (around 10^{-8} A cm^{-2}) and constant with time for all states, which indicates that the material is in a passive state. These values are of the same order of magnitude than those found for other conventional biomaterials [27]. The passive layer formed on the surface by air contact, that according to the XPS results is rich in aluminium oxide, gives the material a high protection against this aggressive environment.

It is also important to evaluate the possibility of passive layer breakdown, that would lead to the formation of pits. The susceptibility to pitting corrosion was evaluated by determining the anodic cyclic polarization

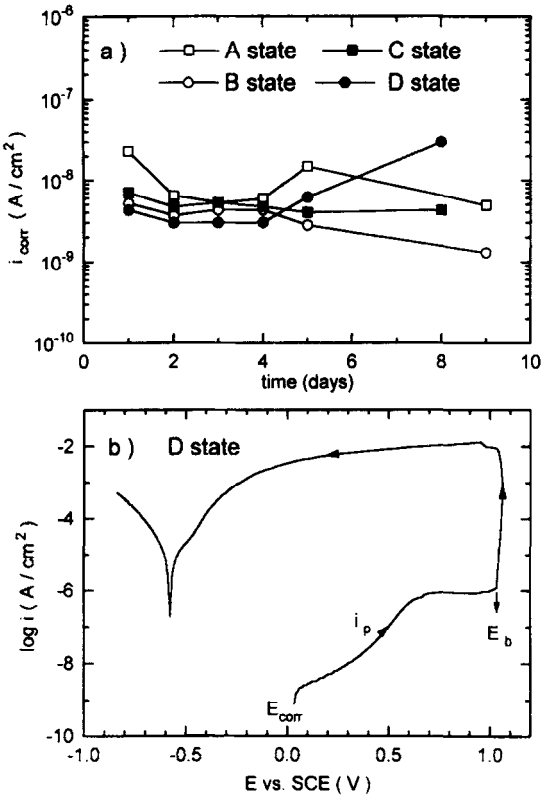

Fig. 4. (a) Corrosion current density, i_{corr} ($A\,cm^{-2}$) vs testing time of immersion in Hank's solution for the different studied alloys: state-A (□), state-B (○), state-C (■) and state-D (●). (B) Anodic cyclic polarization curve for the state-D of the material after 15 days of immersion in Hank's solution

curves. Figure 4(b) represents the anodic cyclic polarization curve of the state-D after 15 days of immersion in Hank's solution because the material in this state is the most important for technological applications. The main parameters that can be obtained from the anodic polarization curves are [28] the corrosion potential, E_{corr}, and the breakdown potential, E_b, as well as the passivation current density, i_p, that are shown in Fig. 4(b). As can be seen, the material shows a passive state with low current density until the breakdown potential is reached. At this point, the current density drastically increases, which is attributed to the activation of a local corrosion process. The high polarization that the material in this state can tolerate, i.e., the difference between E_b and E_{corr}, indicates that the probability of pitting formation is rather low. The susceptibilities to pitting corrosion showed by the other states are widely studied elsewhere [14].

The high corrosion resistance observed for these Fe_3Al-type alloy states is determined mainly by the passive layer formed on the surface. An important fact observed in corrosion studies is that the presence of a mixture of oxides in the passive layer leads to a less corrosion resistant material. Since from the XPS experiments we did not observe Cr at the surface of the studied samples and the Fe oxide content was very low, the high corrosion resistance values observed are determined by the presence of aluminium oxides at the surface.

In summary, we have performed synchrotron radiation PE experiments on four heat-treated Fe_3-Al-type alloy states. The results show a slightly different composition of the passive layer formed in air on the surfaces of all samples. The Al-2*p* PE spectra indicate that the samples have different aluminium oxidation states. The sample in state-D exhibited the highest ratio of Al^{3+} oxidation state to Al^{2+} and Al^{1+}. From the Fe-3*p* and valence band PE experiments it is deduced that the sample with higher Fe-content relative to Al at the surface is the state-C. Electrochemical experiments have shown low corrosion current density values that indicate a very protective passive layer for the four heat-treated samples. The anodic cyclic polarization curve for the D-state alloy shows the high polarization resistance of this sample indicating that the probability of pitting corrosion is quite low. The good corrosion behaviour obtained in Hank's solution permits us to consider this material for room temperature applications, in particular its potential use as biomaterial.

Acknowledgements—The authors thank D.G. Morris and J.L. González-Carrasco for useful discussions. Samples were kindly provided by Shell Laboratories, Arnhem, Holland. Technical assistance by BESSY-staff, especially by T. Kachel is also gratefully acknowledged. This work has been supported by the contract No. CHGE-CT93-0027 of the Human Capital and Mobility Program of the EU and by the project MAT95-0249-C03-01 of the Spanish Comisión Interministerial de Ciencia y Tecnología (CICYT).

REFERENCES

1. Ziegler, N., *AIME Trans.* **100,** 1932, 267.
2. Sykes, C. and Bampfylde, J., *J. Iron and Steel Inst.* **130,** 1934, 389.
3. McKamey, C.G., Horton, J.A. and Liu, C.T., *Scripta Metall. Mater.* **22,** 1988, 1679.
4. McKamey, C.G., Horton, J.A. and Liu, C.T., *J. Mater. Res.* **4,** 1989, 1156.
5. Morris, D.G., Dadras, M.M. and Morris, M.A., *Acta Metall. Mater.* **41,** 1993, 97.
5. McKamey, C.G. and Liu, C.T., *Scripta Metall. Mater.* **24,** 1990, 2119.
6. McKamey, C.G. and Liu, C.T., *Scripta Metall. Mater.* **24,** 1990, 2119.
7. McKamey, C.G. and Pierce, D.H., *Scripta Metall. Mater.* **28,** 1993, 1173.
8. Sun, Z.Q., Huang, Y.D., Yang, W.Y. and Chen, G.L., *Mater. Res. Soc. Symp. Proc.* Vol. 288, p. 885, Mater. Res. Soc., Pittsburgh, 1993.

9. Morris, D.G. and Leboeuf, M., *Acta Metall. Mater.* **42,** 1994, 1817.
10. García-Alonso, M.C., López, M.F., Escudero, M.L., González-Carrasco, J.L. and Morris, D.G., *Scripta Metall. Mater* (submitted).
11. Duquette, D.J., *Intermetallics Compounds: Principles*, Vol. 1, p. 965. Wiley, Chichester (1994).
12. Buchanan, R.A. and Kim, J.G., *Mater. Res. Soc. Symp. Proc.* Vol. 213, p. 945 Mater. Res. Soc., Pittsburgh, 1991.
13. de Cristofaro, N., Frangini, S. and Mignone, A., *Corros. Sci.* **38,** 1996, 307.
14. Frangini, S., de Cristofaro, N.B., Lascovich, J. and Mignone, A., *Corros. Sci.* **35,** 1993, 153.
15. McKamey, C.G., De Van, J.H., Tortorelli, P.F. and Sikka, V.K., *J. Mater. Res.* **6,** 1991, 1779.
16. *Binary Alloys Phase Diagrams* (Edited by T.B. Massalski). ASM, Metals Park, OH, 1986.
17. Vedula, K., *Intermetallics Compounds: Practice*, Vol. 2, p. 199. Wiley, Chichester, 1994.
18. Mears, D.C., *International Metals Reviews*, June, 119, 1977.
19. Stern, M. and Geary, A.L., *J. Electrochem. Soc.* **104,** 1957, 56.
20. Faraci, G., La Rosa, S., Pennisi, A.R., Hwu, Y. and Margaritondo, G., *Phys. Rev.* **B47,** 1993, 4052.
21. Venezia, A.M. and Loxton, C.M., *Surf. Sci.* **194,** 1988, 136.
22. Venezia, A.M., Loxton, C.M. and Horton, J.A., *Surf. Sci.* **225,** 1990, 195.
23. Huttel, Y., Bourdié, E., Soukiassian, P., Mangat, P.S. and Hurych, Z., *J. Vac. Sci. Technol.* **A11,** 1993, 2186.
24. McConville, C.F., Seymour, D.L., Woodruff, D.P. and Bao, S., *Surf. Sci.* **188,** 1987, 1.
25. Penn, D.R., *Phys. Rev.* **B13,** 1976, 5248.
26. Kato, H., Ishii, T., Masuda, S., Harada, Y., Miyano, T., Komeda, T., Onchi, M. and Sakisaka, Y., *Phys. Rev.* **B32,** 1985, 1992.
27. Escudero, M.L., López, M.F., Ruiz, J., García-Alonso, M.C. and Canahua, H., *J. Biomed. Mater. Res.* (in print).
28. Escudero, M.L., González, J.A. and Ruiz, J., *Werkst. Korros.* **39,** 1988, 364.